

Crack localization by laser-induced narrowband ultrasound and nonlinear ultrasonic modulation

Peipei Liu, Jinho Jang and Hoon Sohn*

Department of Civil and Environmental Engineering, Korean Advanced Institute for Science and Technology,
291 Daehak-ro, Yuseong-gu, Daejeon 34141, Republic of Korea

(Received October 30, 2019, Revised December 24, 2019, Accepted December 27, 2019)

Abstract. The laser ultrasonic technique is gaining popularity for nondestructive evaluation (NDE) applications because it is a noncontact and couplant-free method and can inspect a target from a remote distance. For the conventional laser ultrasonic techniques, a pulsed laser is often used to generate broadband ultrasonic waves in a target structure. However, for crack detection using nonlinear ultrasonic modulation, it is necessary to generate narrowband ultrasonic waves. In this study, a pulsed laser is shaped into dual-line arrays using a spatial mask and used to simultaneously excite narrowband ultrasonic waves in the target structure at two distinct frequencies. Nonlinear ultrasonic modulation will occur between the two input frequencies when they encounter a fatigue crack existing in the target structure. Then, a nonlinear damage index (DI) is defined as a function of the magnitude of the modulation components and computed over the target structure by taking advantage of laser scanning. Finally, the fatigue crack is detected and localized by visualizing the nonlinear DI over the target structure. Numerical simulations and experimental tests are performed to examine the possibility of generating narrowband ultrasonic waves using the spatial mask. The performance of the proposed fatigue crack localization technique is validated by conducting an experiment with aluminum plates containing real fatigue cracks.

Keywords: fatigue crack localization; laser scanning; laser ultrasonic; narrowband excitation; nonlinear ultrasonic modulation; spatial mask

1. Introduction

The laser ultrasonic technique is gaining popularity for nondestructive evaluation (NDE) applications because of its versatility. The laser ultrasonic technique allows inspection of moving objects (Park *et al.* 2013) and micro devices (Hurley *et al.* 2001), inspection in extremely harsh (hot (Dewhurst *et al.* 1988), cold (Mikesell *et al.* 2017) or underwater (Pistone *et al.* 2013)) environments, and long range inspection of areas that are difficult to reach (Yang *et al.* 2015, Park *et al.* 2017). The laser ultrasonic technique consists of ultrasonic generation and sensing. When a laser beam is directed at a target structure, localized heating of the surface causes thermoelastic expansion of the material and creates ultrasonic waves (Scruby and Drain 1990). Laser ultrasonic generation has been achieved using a pulsed laser (Davies *et al.* 1993), a modulated continuous-wave laser (Pierce *et al.* 1998, Prada *et al.* 2005) or laser arrays (Deaton *et al.* 1990, Noroy *et al.* 1995). Laser ultrasonic sensing has been performed using a laser interferometer (Monchalain *et al.* 1989) or laser Doppler vibrometer (LDV) (Staszewski *et al.* 2004, An *et al.* 2013a) and by measuring the reflectivity change caused by ultrasound-induced strain (Saito *et al.* 2010). The excitation and sensing lasers can further incorporate scanning mirrors

so that wavefield images with a high spatial resolution can be constructed (An *et al.* 2013a).

Fatigue cracks have been detected by line scanning a pulsed laser excitation over metal sheets and measuring the ultrasonic responses with an electromagnetic acoustic transducer (EMAT) (Dixon *et al.* 2011). The interaction between ultrasonic waves and cracks was observed from ultrasonic wavefield images obtained by scanning a pulsed laser excitation and employing a fixed contact-type transducer for sensing (Yashiro *et al.* 2008). Similar ultrasonic wave propagation images were constructed by scanning a sensing laser interferometer (or LDV) and a fixed piezoceramic actuator or a pulsed laser for the excitation (Staszewski *et al.* 2007, An *et al.* 2013b).

The aforementioned techniques rely on linear features such as variations in the amplitude, phase, and mode conversion of ultrasonic waves either transmitted or reflected from a crack. It has been reported that the changes in these linear features become prominent only when a fatigue crack grows towards the intermediate and end stages (phase II and III in the stress-life (S-N) curve) of the useful fatigue life (Jhang 2009). Because a fatigue crack grows at an alarming rate once the crack size reaches the intermediate and end stages of the fatigue life, it is important to detect a fatigue crack in its early stage.

Recent studies have shown that a fatigue crack and its precursor often serve as a source for generating nonlinear waves such as the accompanying harmonics, modulations between different frequencies, and resonance frequency

*Corresponding author, Professor,
E-mail: hoonsohn@kaist.ac.kr

shifts as a function of the input amplitude (Jhang 2009). The sensitivity of the extracted nonlinear features to a fatigue crack has been shown to be much higher than that which can be achieved with linear features (van den Abeele *et al.* 2000, Yim *et al.* 2016, Lim *et al.* 2017). Among the different nonlinear ultrasonic techniques, the nonlinear ultrasonic modulation technique has been shown to be less influenced by the unwanted nonlinearity of data acquisition systems. A pair of air-coupled transducers (ACTs) was used to generate two distinct frequency inputs, and the responses were scanned with an LDV for fatigue crack detection based on nonlinear ultrasonic modulation (Lim *et al.* 2015). Alternatively, the intensities of two continuous-wave lasers can be modulated to generate ultrasonic waves at two distinct frequencies for nonlinear ultrasonic modulation (Mezil *et al.* 2016). In addition, various signal processing methods have been proposed to extract nonlinear modulation features from broadband ultrasonic responses induced by a pulsed laser (Liu *et al.* 2015, 2018).

This paper uses the irradiation pattern of a line array to generate narrowband ultrasonic waves from a pulsed laser and develops a fatigue crack detection and localization technique based on nonlinear interaction between two laser-induced narrowband ultrasonic waves. The uniqueness and advantages of the proposed technique include the following: (1) the effects of the line laser array on the dispersion and multimodal characteristics of the generated narrowband ultrasonic waves in a plate-like structure are numerically and experimentally investigated; (2) a spatial mask with dual-line arrays is designed to simultaneously generate two narrowband ultrasonic waves with distinct central frequencies; (3) using two narrowband ultrasonic waves, the nonlinear ultrasonic modulation created by a fatigue crack in a target structure is identified; and (4) through synchronized scanning of both the excitation and sensing laser beams, the fatigue crack is detected and localized.

The rest of this paper is organized as follows. Section 2 numerically and experimentally investigates whether a line laser array can effectively generate narrowband ultrasonic waves. Section 3 describes the nonlinear ultrasonic modulation phenomenon between two laser-induced narrowband ultrasonic waves and develops a fatigue crack localization technique. In Section 4, the test results from aluminum plates with fatigue cracks are presented and discussed. Finally, a conclusion is provided in Section 5.

2. Narrowband ultrasonic generation using a line laser array

2.1 Numerical simulation

An equivalent 2D plane strain model of a 3-mm-thick aluminum plate was designed using the commercial finite element software COMSOL Multiphysics. As shown in Fig. 1, the x -axis denotes the wave propagation direction along the plate, whereas the y -axis represents the plate thickness direction. The material properties of the aluminum used for the simulation are listed in Table 1. When the plate is illuminated by a pulsed laser, the surface of the plate absorbs the electromagnetic radiation from the laser, and the

resulting thermal conduction can be expressed as follows (Xu *et al.* 2004)

$$\rho C_p \frac{\partial T(x, y, t)}{\partial t} = \nabla(k \nabla T(x, y, t)) + Q \quad (1)$$

Where $T(x, y, t)$ represents the time-dependent temperature variation along the x and y directions. ρ , C_p and k are the density, specific heat capacity at a constant pressure, and thermal conductivity, respectively. In this model, the pulsed laser is treated as a heat flux and applied onto the top surface of the plate at $x = 0$. When the laser is treated as a heat flux rather than a heat source ($Q = 0$), Eq. (1) can be simplified as

$$\rho C_p \frac{\partial T(x, y, t)}{\partial t} = \frac{1}{x} \frac{\partial}{\partial x} \left(x k \frac{\partial T(x, y, t)}{\partial x} \right) + \frac{\partial}{\partial y} \left(k \frac{\partial T(x, y, t)}{\partial y} \right) \quad (2)$$

The normal boundary conditions are as follows

$$\begin{aligned} -k \frac{\partial T(x, y, t)}{\partial y} \Big|_{y=0} &= I f(x) g(t) \\ \frac{\partial T(x, y, t)}{\partial y} \Big|_{y=h} &= 0 \end{aligned} \quad (3)$$

where I is the peak power intensity of the pulsed laser, and $f(x)$ and $g(t)$ are the spatial and temporal distributions of the laser, respectively. h is the thickness of the plate. The spatial distribution of the laser, $f(x)$, has 6 parallel lines with a gap of λ (Fig. 1). Note that λ dominates the wavelength of the generated ultrasonic waves in the plate.

The thermal conduction produced by the pulsed laser generates thermal waves in the plate and consequently ultrasonic waves. For a typical Q-switched pulsed laser (12 ns pulse duration in this simulation), the induced thermal waves can propagate only a few micrometers from the laser source, even in highly conductive materials (Scruby and Drain 1990). This thermal wave region results in a stress redistribution and produces a transient displacement field

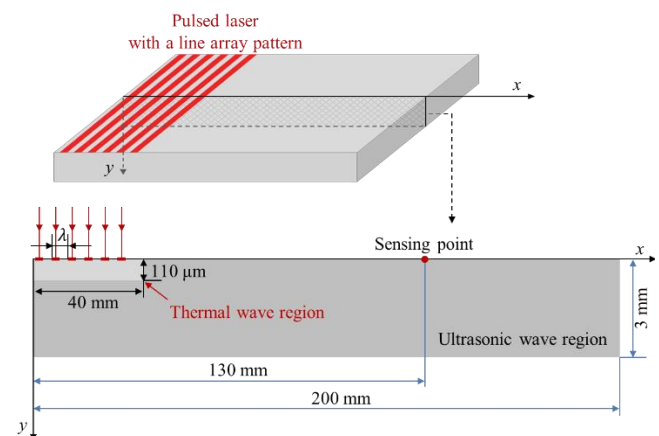


Fig. 1 Schematic of a 2D FEM plate model irradiated by a line laser array

Table 1 Material properties of the aluminum used for the numerical simulation

Density ρ (kg/m ³)	Young's modulus E (GPa)	Poisson's ratio ν	Coefficient of thermal expansion α_t (K ⁻¹)	Thermal conductivity K (W/(m·K))	Heat capacity at constant pressure C_p (J/(kg·K))
2700	68.9	0.33	2.34×10^{-5}	170	900

(ultrasonic wave region) throughout the plate, as illustrated in Fig. 1. In an aluminum plate, the displacement satisfies (Xu *et al.* 2004)

$$(\lambda + 2\mu)\nabla(\nabla \cdot \mathbf{U}(x, y, t)) - \mu\nabla \times \nabla \times \mathbf{U}(x, y, t) - \alpha_t(3\lambda + 2\mu)\nabla T(x, y, t) = \rho \frac{\partial^2 \mathbf{U}(x, y, t)}{\partial t^2} \quad (4)$$

where $\mathbf{U}(x, y, t)$ is the time-dependent displacement, λ and μ are the Lamé constants, and α_t is the thermoelastic expansion coefficient of the material. To enhance the computational efficiency, a multiscale element strategy was used for the thermal and ultrasonic wave regions. A detailed explanation of the multiscale element strategy can be found in Liu and Sohn (2016). Within the thermal wave region, one thermal degree of freedom and two mechanical degrees of freedom are assumed for each node of the element. Within the ultrasonic wave region, each node has only two mechanical degrees of freedom.

In the simulation, the line gap λ of the input line laser array was varied from 1 mm to 2, 2.6, 3, 4 and 5 mm. A uniform heat flux with a power intensity of 2.5×10^5 MW/m² was assumed within the laser illumination area for 12 ns. The initial temperature and displacement field values at $t = 0$ were set to $T = 293.15$ K and $\mathbf{U} = (0, 0)$, respectively. The simulation was performed for 150 μ s with a time step of 1 ns for the first 12 ns and 200 ns for the rest of the simulation.

Taking $\lambda = 2.6$ and 4 mm as examples, Fig. 2 shows the time histories of the temperature variation on the top surface along the x direction. It is observed that the temperature increase is confined within the line array area where the simulated laser heat flux is exerted. Fig. 3 shows the out-of-plane (along the y direction) velocity signals and the corresponding frequency responses measured at the sensing point in Fig. 1. Due to the dispersion and multimodal characteristics of ultrasound in a thin plate, two dominant wave packages with different central frequencies

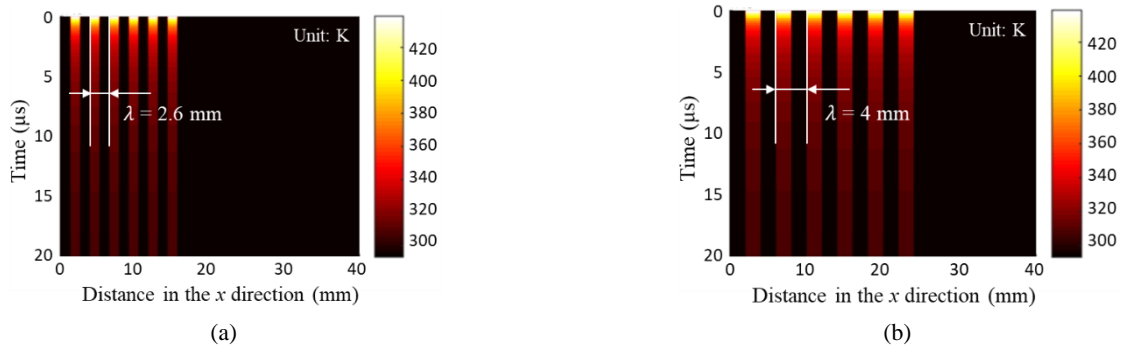


Fig. 2 Temporal and spatial profiles (on the top surface, $y = 0$) of the temperature response irradiated by a line laser array with (a) $\lambda = 2.6$ mm; and (b) $\lambda = 4$ mm

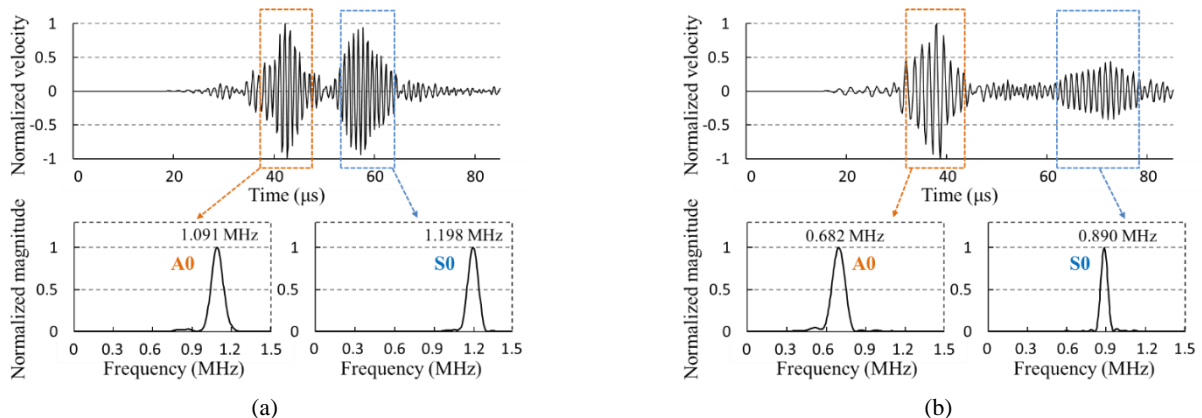


Fig. 3 Velocity signals generated in the numerical simulation by a line laser array with (a) $\lambda = 2.6$ mm; and (b) $\lambda = 4$ mm

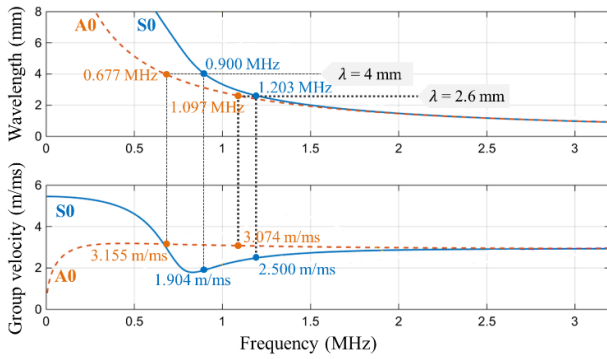


Fig. 4 Dispersion curves with respect to wavelength and group velocity for a 3-mm-thick aluminum plate

are identified in Fig. 3.

Fig. 4 shows the dispersion curves with respect to wavelength and group velocity for a 3-mm-thick aluminum plate. Here, only the zero-order wave modes are shown for simplicity. As mentioned above, the value of λ determines the wavelength of the generated ultrasonic waves. When $\lambda = 2.6$ mm, zero-order antisymmetric (A0) and symmetric (S0) wave modes are generated at 1.097 and 1.203 MHz, respectively, as plotted in Fig. 4. These frequencies are in good agreement with those (1.091 MHz for the A0 wave mode and 1.198 MHz for the S0 wave mode) estimated from the simulation shown in Fig. 3(a). Additionally, the group velocities of the A0 and S0 wave modes (3.074 m/ms for the A0 wave mode and 2.500 m/ms for the S0 wave mode) shown in Fig. 4 match well with the arrival times of the two wave packages shown in Fig. 3(a) (3.059 m/ms estimated for the A0 wave mode and 2.378 m/ms for the S0 wave mode). Similar trends can be found when $\lambda = 4$ mm, as shown in Figs. 3(b) and 4. The simulations illustrate that narrowband ultrasonic waves can be effectively generated using a line laser array. Moreover, it has been reported that the signal-to-noise ratio for laser-induced ultrasonic waves can be improved using a line laser array for the excitation (Wagner *et al.* 1990). The frequencies of the A0 and S0 wave modes obtained from both analytical dispersion curves and numerical simulations are summarized in Table 2 and Fig. 5 for $\lambda = 1, 2, 2.6, 3, 4$ and 5 mm.

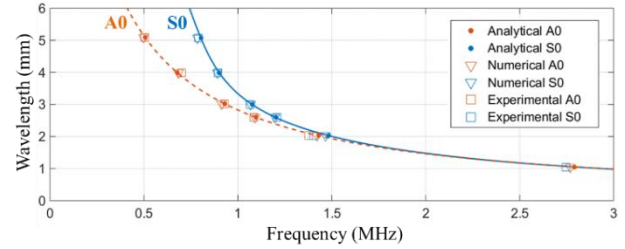


Fig. 5 Analytical, numerical and experimental dispersion curves corresponding to various wavelengths (line gaps), $\lambda = 1, 2, 2.6, 3, 4$ and 5 mm

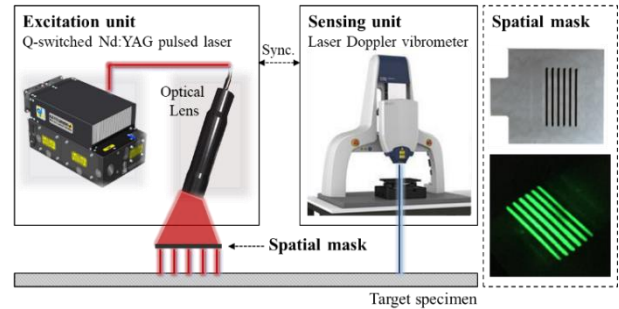


Fig. 6 Experimental setup for narrowband ultrasonic generation with a custom-made spatial mask

2.2 Experimental validation

To experimentally validate the effect of the line laser array on ultrasonic generation, a 3-mm-thick circular aluminum plate with a radius of 150 mm was prepared. Fig. 6 shows an overview of the experimental setup. The excitation was applied at the center of the aluminum plate, and the sensing point was located 130 mm away from the center. A diode pumped Q-switched Nd:YAG pulsed laser (Quantel Centurion+) was used for the excitation. The Nd:YAG pulsed laser has a wavelength of 532 nm, a pulse duration of 12 ns and a maximum pulse energy of 25 mJ. In this experiment, a pulse energy of approximately 20 mJ was used, and an optical lens was installed in front of the pulsed laser. The optical lens adjusts the laser beam size and aims the laser beam at a custom-made spatial mask. Here, the spatial mask illuminates the target surface with a desired

Table 2 Comparison of the A0 and S0 wave mode frequencies obtained by the analytical dispersion curve, numerical simulation and experiment

λ (mm)	Frequency components (MHz)					
	Dispersion curve		Numerical simulation		Experiment	
	A0	S0	A0	S0	A0	S0
1	2.790	2.790	2.768	2.768	2.745	2.745
2	1.464	1.482	1.421	1.467	1.376	1.403
2.6	1.097	1.203	1.091	1.198	1.086	1.207
3	0.930	1.077	0.914	1.069	0.927	1.065
4	0.677	0.900	0.682	0.890	0.701	0.893
5	0.507	0.803	0.498	0.783	0.504	0.789

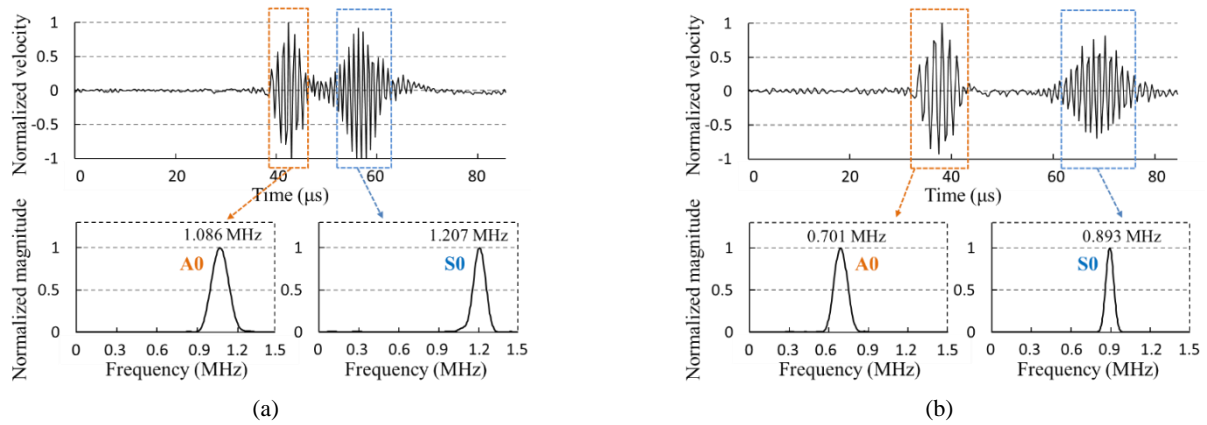


Fig. 7 Ultrasonic responses obtained in the experiment by a line laser array with (a) $\lambda = 2.6$ mm; and (b) $\lambda = 4$ mm

shape (Wagner *et al.* 1990, Baldwin *et al.* 1999). This custom-made spatial mask, made of polyether ether ketone (PEEK), has 6 parallel line patterns identical to those in the simulation. The gap between two adjacent line patterns illuminated on the aluminum plate, λ , can be adjusted by changing the distance between the optical lens / spatial mask and the plate surface. Identical to the simulation, line laser array excitations with $\lambda = 1, 2, 2.6, 3, 4$ and 5 mm were tested. Note that line laser array patterns can also be created by adopting multiple laser sources (Murray *et al.* 1996) or using diffractive optical elements (DOEs) (Huang *et al.* 1992). The out-of-plane ultrasonic responses at the sensing point were measured by a commercial LDV (Polytec MSA-100) with a sampling frequency of 6.25 MHz for $150 \mu\text{s}$. To improve the signal-to-noise ratio, the responses were measured 100 times and averaged in the time domain.

Figs. 7(a) and (b) show the velocity responses corresponding to $\lambda = 2.6$ and 4 mm in the time and frequency domains, respectively. The comparison of the simulation and experimental results in Figs. 3 and 7 shows that, using a spatial mask, narrowband ultrasonic waves can be effectively generated, and their central frequencies can be controlled by adjusting λ . Note that the difference between the time-domain signals in Figs. 3 and 7 is mainly attributed to the fact that the length of the parallel laser lines is infinite in the simulation while it is limited and finite in the experiment. The central frequencies of the A0 and S0 wave modes obtained by the experiment are summarized in Table 2 and Fig. 5. Good agreement can be found among the frequencies obtained from analytical dispersion curves, numerical simulations and experiments.

3. Fatigue crack detection using dual-line laser arrays

3.1 Generation of nonlinear ultrasonic modulation using dual-line laser arrays

Nonlinear ultrasonic modulation has been shown to be an effective indicator of fatigue crack formation at its early stage, assuming that the inherent material nonlinearity is weak and negligible (Zaitsev *et al.* 2009). Normally, two

sinusoidal ultrasonic inputs with distinct frequencies are applied to a target structure for nonlinear modulation inspection. When the structure is intact (linear), the structural response contains frequency components only at the input frequencies. Once the structure is damaged, the response will include not only the input frequency components but also their harmonics (multiples of the input frequencies) and modulations (linear combinations of the two input frequencies) (Zaitsev *et al.* 2009). Note that the generation of nonlinear ultrasonic modulation needs to satisfy certain conditions that depend on the selection of the two ultrasonic inputs. The conditions can be summarized as follows (Lim *et al.* 2014, Lim and Sohn 2017): (1) the strain (displacement) at the damage location should oscillate in response to both inputs; and (2) the motion induced by one of the two inputs should modulate the other input at the damage location. Although both the A0 and S0 wave modes will be generated in the aluminum plate when using a line laser array for the excitation, only the S0 wave mode can satisfy the conditions for the generation of nonlinear ultrasonic modulation in a plate-like structure (Lim and Sohn 2017). Therefore, only the induced S0 wave mode will be considered for the following fatigue crack detection.

3.2 Fatigue crack detection using nonlinear ultrasonic modulation

By taking advantage of the narrowband ultrasonic waves induced by dual-line laser arrays, a nonlinear ultrasonic modulation technique is developed. As shown in Fig. 8, the dual-line laser arrays consist of two line laser arrays with different line gaps. In Fig. 8, the A0 wave mode and higher-order modes are omitted for simplicity. When dual-line laser arrays with line gaps of λ_1 and λ_2 are illuminated on a target structure, S0 wave modes with central frequencies f_1 and f_2 will be generated. Then, nonlinear ultrasonic modulation between these two S0 wave modes will occur when these modes encounter a fatigue crack at the same time. Finally, the fatigue crack is identified by detecting the crack-induced nonlinear modulation components.

Analogous to the classic nonlinear index (van den Abeele *et al.* 2000), a nonlinear damage index (DI) is defined here by considering the modulation component at $f_2 - f_1$

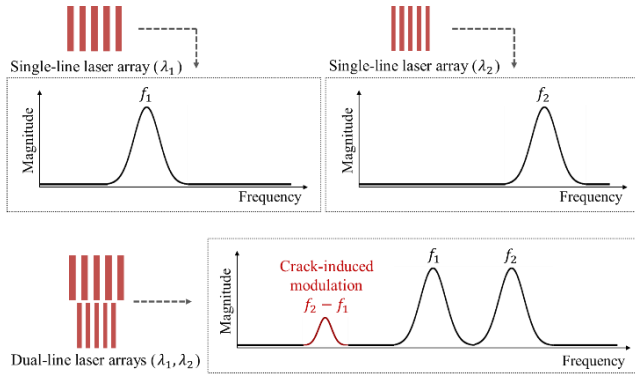


Fig. 8 Generation of two narrowband ultrasonic waves and crack-induced modulation components using dual-line laser arrays

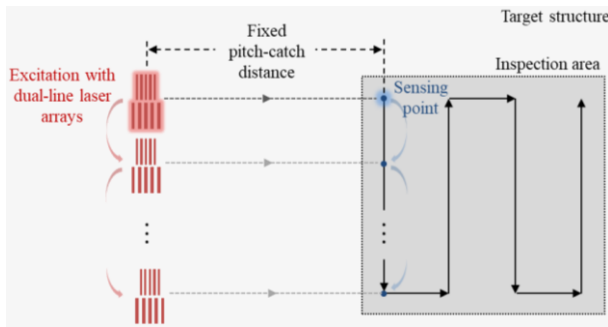


Fig. 9 Synchronized laser scanning with dual-line laser arrays used for the excitation

$$DI = \frac{A_{f_2 - f_1}}{A_{f_1} A_{f_2}} \quad (5)$$

where A_{f_1} and A_{f_2} are the amplitudes of the linear responses at f_1 and f_2 , respectively, and $A_{f_2 - f_1}$ is the amplitude of the modulation component at $f_2 - f_1$. The DI can be interpreted as the amplitude of the modulation component normalized by the product of the responses at the input frequencies. Note that among the various modulation components, only the first-order modulation component at $f_2 - f_1$ is considered in this study because the other modulation components (e.g., $f_2 + f_1$) may overlap with higher-order modes in the frequency domain.

3.3 Fatigue crack localization using synchronized laser scanning

As shown in Fig. 9, a fatigue crack is localized by simultaneously scanning the excitation and sensing laser beams with a fixed pitch-catch distance over the entire inspection area. The dual-line laser arrays are adopted for generating two S0 wave modes with different central frequencies, and the corresponding response is measured at the sensing point using a sensing laser. As each sensing point, the resulting time response is stored, and the proposed DI value is computed. By controlling the gap between two sequential sensing points, the spatial resolution of the scanning process can be adjusted. Here, the layout of

the dual-line laser arrays and the pitch-catch distance are selected so that the mixing of the two S0 wave modes can occur only at the sensing point and hence a fatigue crack can be localized by searching for relatively large DI values within the inspection area. The proposed scanning strategy does not require any baseline data obtained from the intact condition and minimizes the false alarms caused by varying operational and environmental conditions (Liu *et al.* 2015).

4. Experimental validation

4.1 Experimental setup

To examine the performance of the proposed fatigue crack localization technique, three 3-mm-thick aluminum plate specimens, fabricated using 6061-T6 aluminum alloy, were prepared. All the geometrical information of the specimen can be found in Fig. 10(a). A notch was introduced in the middle of one edge of the specimen so that a fatigue crack could initiate from this notch. Cyclic loading tests were carried out using a universal testing machine (INSTRON 8801) with a 10 Hz cycle rate, a maximum load of 25 kN, and a stress ratio of 0.1 to initiate a fatigue crack from the notch in two specimens, named D1 and D2. The introduced fatigue cracks are approximately 15 mm long. The crack width is less than 15 μm near the crack tip and less than 50 μm overall (Fig. 10(b)). The remaining intact specimen is labeled I1.

The measurement system is identical to the one presented in Section 2. The only difference is that a spatial mask with dual-line arrays was used, as shown in Fig. 11. The dual-line laser arrays in this experiment direct the pulsed laser to the target surface with two different line gaps, $\lambda_1 = 4$ mm and $\lambda_2 = 2.6$ mm. The layout of the dual-line laser arrays and the distance from the sensing point were selected to be approximately 45 mm so that the two induced S0 wave modes could simultaneously arrive at the sensing point, as shown in Fig. 10(a). A 5 mm \times 5 mm square area shown in Fig. 10(a) was defined as the target inspection area covering the fatigue crack tip. A total of 400 (20 \times 20) sensing points were assigned within this inspection area, achieving a spatial resolution of 0.25 mm. In this experiment, scanning was realized by placing the specimens on an XY-positioning table integrated into the sensing LDV (Polytec MSA-100). The rest of the experimental setup is identical to that in Section 2.

4.2 Test results

First, the responses obtained from two separate single-line laser arrays with $\lambda_1 = 4$ mm and $\lambda_2 = 2.6$ mm are plotted for the intact specimen (I1) in Figs. 12(a) and (b), respectively. The induced S0 wave modes in Fig. 12(a) and (b) have central frequencies of 0.896 MHz and 1.209 MHz, respectively, and almost simultaneously arrive at the sensing point. In Fig. 12(c), the two S0 wave modes are simultaneously generated using dual-line laser arrays.

Fig. 13 compares the responses obtained from an intact sensing point far from the crack tip (Fig. 13(a)) and another sensing point near the crack tip (Fig. 13(b)) of the damaged

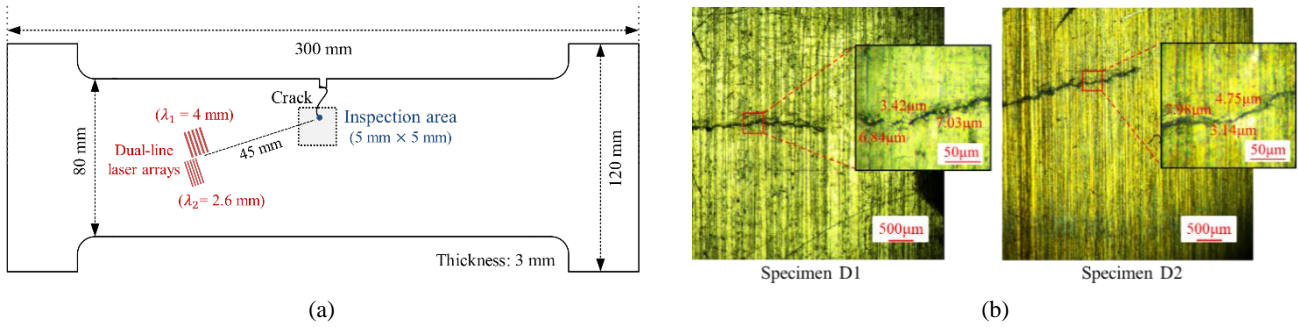


Fig. 10 Description of the target aluminum plates: (a) geometric dimensions, crack location, and laser excitation and sensing arrangement; and (b) microscopic images of the fatigue crack tips within the selected inspection area

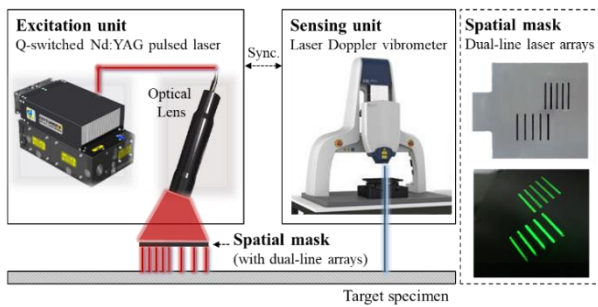


Fig. 11 Experimental setup for laser scanning with dual-line laser arrays used for the excitation

specimen, D1. A comparison between Figs. 13(a) and (b) reveals that the amplitude of the nonlinear modulation component is large when the sensing point is near the fatigue crack. Because of the test-to-test fluctuation of the S0 mode central frequencies, the central frequencies of the induced S0 wave modes are first estimated, and the amplitude at the estimated modulation frequency is computed afterwards.

The nonlinear DI value, as defined in Eq. (5), was then calculated for all the sensing points in the target inspection area. The corresponding fatigue crack localization results are shown in Fig. 14 for all three specimens. High DI values appear mostly along the crack, and it is speculated that the

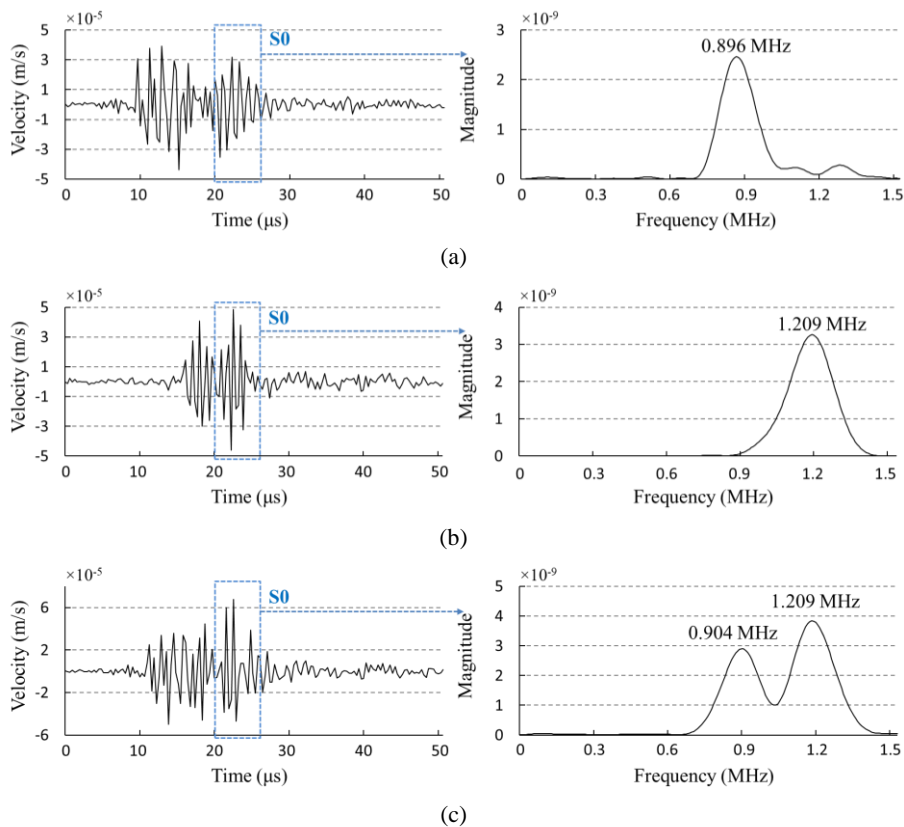


Fig. 12 Representative ultrasonic signals obtained with (a) a single-line laser array with $\lambda_1 = 4$ mm; (b) a single-line laser array with $\lambda_2 = 2.6$ mm; and (c) dual-line laser arrays with $\lambda_1 = 4$ mm and $\lambda_2 = 2.6$ mm (from the intact specimen, II)

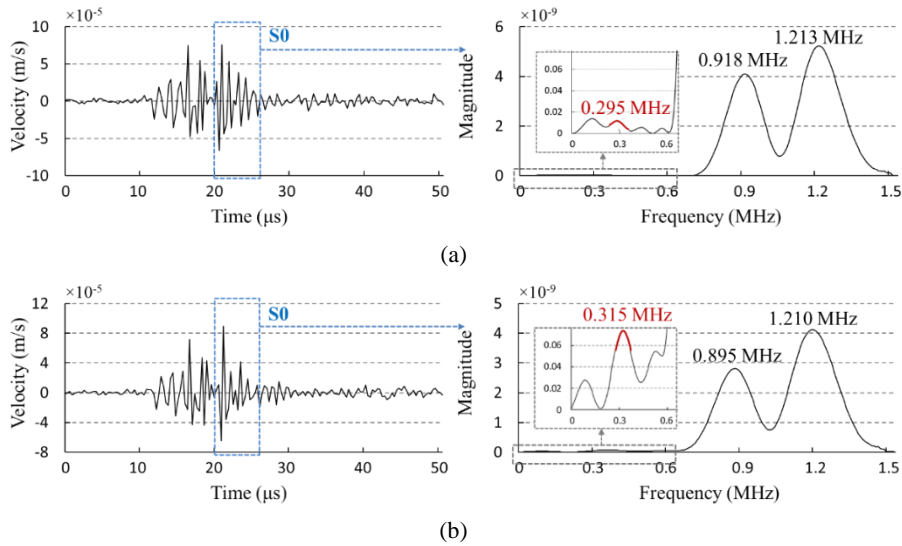


Fig. 13 Representative ultrasonic signals obtained from (a) an intact sensing hpgpoint and (b) a sensing point near the crack (from the damaged specimen, D1)

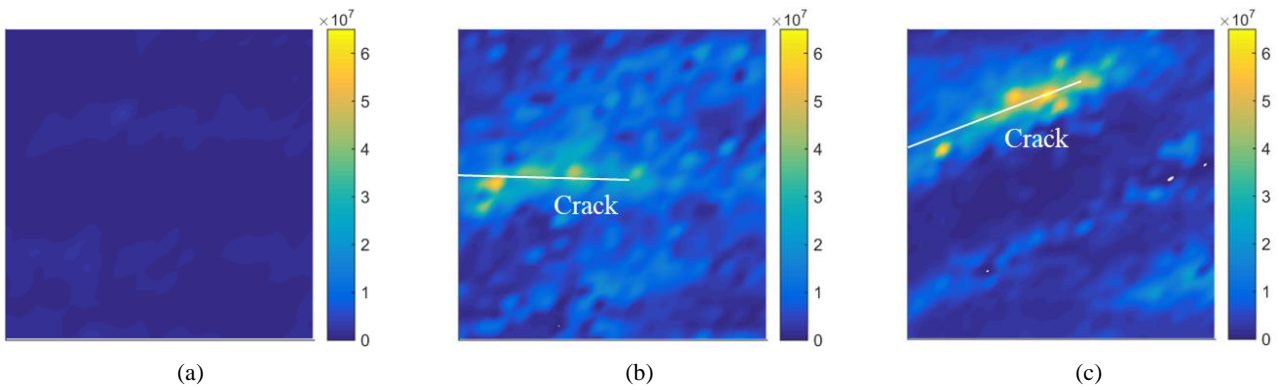


Fig. 14 Fatigue crack detection results using the proposed nonlinear DI: (a) I1; (b) D1; and (c) D2

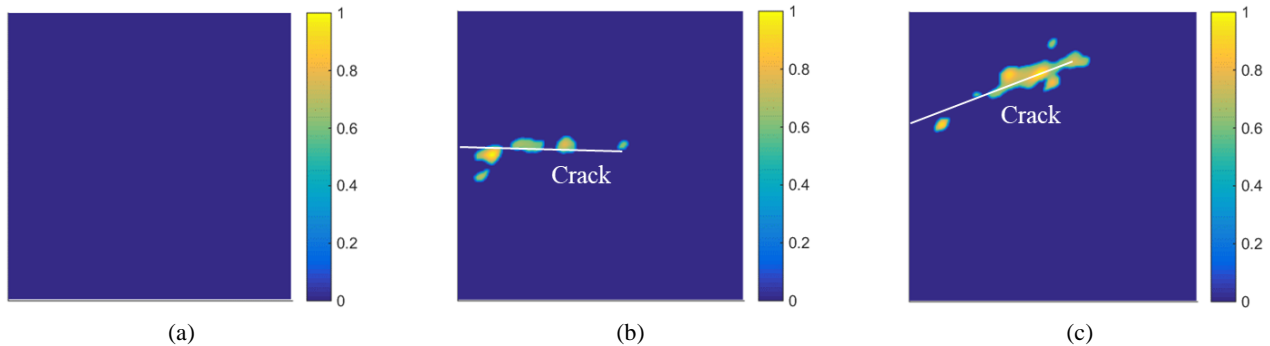


Fig. 15 Fatigue crack localization results after signal/image processing: (a) I1; (b) D1; and (c) D2. A sequential outlier analysis was applied to the results in Fig. 14. The DI values of the identified outliers were normalized with respect to the largest DI values, and the remaining DI values, which were not classified as the outliers, were set to zero

DI values are large where the crack opening and closing is severe.

Further signal/image processing can be introduced to improve and automate the fatigue crack detection and localization. For example, a sequential outlier analysis is introduced in this experiment (Liu *et al.* 2014, Sohn *et al.* 2007). The basic premise is that the DI values from sensing

points located near the fatigue crack will be significantly larger than the DI values obtained from the intact sensing points. First, all the DI values within the inspection area were arranged in ascending order. Second, a normal distribution was fitted to the first (smallest) half of the DI values (the 200 smallest DI values among 400 DI values in this experiment). Here, it was assumed that the first half of

the DI values were obtained from the sensing points far from a fatigue crack. Third, a threshold corresponding to a 99% confidence interval was established from the fitted normal distribution. Fourth, if the 201st smallest DI value was larger than the threshold, the 201st smallest DI values and all the other larger DI values would be classified as outliers. Otherwise, the above procedure was repeated by including the 201st smallest DI value into the fitting of a new normal distribution and testing if the next (202nd in this experiment) smallest DI value was an outlier or not. This outlier process was repeated until the outlier(s) were detected or the largest DI value was tested. In the end, the DI values of the identified outliers were normalized with respect to the largest DI values, and the remaining DI values, which were not classified as outliers, were set to zero. The results of the image processing are shown for specimens I1, D1 and D2 in Fig. 15.

5. Conclusions

In this study, a noncontact fatigue crack localization technique is developed using dual-line laser arrays and nonlinear ultrasonic modulation. First, two narrowband ultrasonic waves with distinct central frequencies are generated using dual-line laser arrays. Here, the central frequency of each narrowband ultrasonic wave is controlled by adjusting the line spacing, and the dual-line laser arrays are designed so that the mixing of these two ultrasonic waves occurs at the sensing point. Then, the excitation and sensing laser beams are scanned simultaneously with a fixed pitch-catch distance over the entire inspection area, and the fatigue crack is identified by extracting the nonlinear ultrasonic modulation components induced by the crack. The uniqueness and advantages of the proposed technique are as follows: (1) the effects of the line laser array on the dispersion and multimodal characteristics of the generated narrowband ultrasonic waves are numerically and experimentally investigated; (2) a spatial mask with dual-line arrays is designed to simultaneously generate two narrowband ultrasonic waves with distinct central frequencies; (3) using two narrowband ultrasonic waves, the nonlinear ultrasonic modulation created by the fatigue crack in an aluminum plate is identified; and (4) through synchronized scanning of both the excitation and sensing laser beams, the fatigue crack is detected and localized.

The performance of the proposed technique is examined by detecting microscale fatigue cracks in aluminum plate specimens. The average length of these fatigue cracks is approximately 15 mm, and their width is less than 15 μm within the selected inspection area. Note that the minimum wavelength of the narrowband ultrasonic waves generated in this study is limited to the mm-scale, but this limitation can be overcome by using DOEs. A future study is warranted to generate various laser illumination patterns using DOEs, study their effects on ultrasonic generation, and apply the proposed technique to various targets such as silicon wafers.

Acknowledgments

This work was supported by a National Research Foundation of Korea (NRF) grant funded by the Korea government (MSIT) (No. 2019R1C1C1009493), and also a National Research Foundation of Korea (NRF) grant funded by the Korea government (MSIT) (No. 2019R1A3B3067987).

References

- An, Y.K., Park, B. and Sohn, H. (2013a), "Complete noncontact laser ultrasonic imaging for automated crack visualization in a plate", *Smart Mater. Struct.*, **22**(2), 025022. <https://doi.org/10.1088/0964-1726/22/2/025022>.
- An, Y.K., Kwon, Y. and Sohn, H. (2013b), "Noncontact laser ultrasonic crack detection for plates with additional structural complexities", *Struct. Health Monit.*, **12**(5-6), 522-538. <https://doi.org/10.1177/1475921713500515>
- Baldwin, K.C., Berndt, T.P. and Ehrlich, M.J. (1999), "Narrowband laser generation/air-coupled detection: Ultrasonic system for on-line process control of composites", *Ultrasonics*, **37**(5), 329-334. [https://doi.org/10.1016/S0041-624X\(99\)00011-6](https://doi.org/10.1016/S0041-624X(99)00011-6)
- Davies, S., Edwards, C., Taylor, G. and Palmer, S.B. (1993), "Laser-generated ultrasound: Its properties, mechanisms and multifarious applications", *J. Phys. D Appl. Phys.*, **26**(3), 329-348. <https://doi.org/10.1088/0022-3727/26/3/001>
- Deaton Jr, J., McKie, A., Spicer, J. and Wagner, J. (1990), "Generation of narrow-band ultrasound with a long cavity mode-locked Nd: YAG laser", *Appl. Phys. Lett.*, **56**(24), 2390-2392. <https://doi.org/10.1063/1.102925>
- Dewhurst, R.J., Edwards, C., McKie, A.D.W. and Palmer, S.B. (1988), "A remote laser system for ultrasonic velocity measurement at high temperatures", *J. Appl. Phys.*, **63**(4), 1225-1227. <https://doi.org/10.1063/1.339987>
- Dixon, S., Burrows, S., Dutton, B. and Fan, Y. (2011), "Detection of cracks in metal sheets using pulsed laser generated ultrasound and EMAT detection", *Ultrasonics*, **51**(1), 7-16. <https://doi.org/10.1016/j.ultras.2010.05.002>
- Huang, J., Krishnaswamy, S. and Achenbach, J.D. (1992), "Laser generation of narrow-band surface waves", *J. Acoust. Soc. Amer.*, **92**(5), 2527-2531. <https://doi.org/10.1121/1.404422>
- Hurley, D.C., Tewary, V.K. and Richards, A.J. (2001), "Thin-film elastic-property measurements with laser-ultrasonic SAW spectrometry", *Thin Solid Films*, **398-399**, 326-330. [https://doi.org/10.1016/S0040-6090\(01\)01338-4](https://doi.org/10.1016/S0040-6090(01)01338-4)
- Jhang, K.Y. (2009), "Nonlinear ultrasonic techniques for nondestructive assessment of micro damage in material: A review", *International J. Precis. Eng. Manuf.*, **10**(1), 123-135. <https://doi.org/10.1007/s12541-009-0019-y>
- Lim, H.J. and Sohn, H. (2017), "Necessary conditions for nonlinear ultrasonic modulation generation given a localized fatigue crack in a plate-like structure", *Materials*, **10**(3), 248. <https://doi.org/10.3390/ma10030248>
- Lim, H.J., Sohn, H. and Liu, P. (2014), "Binding conditions for nonlinear ultrasonic generation unifying wave propagation and vibration", *Appl. Phys. Lett.*, **104**(21), 214103. <https://doi.org/10.1063/1.4879836>
- Lim, H.J., Song, B., Park, B. and Sohn, H. (2015), "Noncontact fatigue crack visualization using nonlinear ultrasonic modulation", *NDT & E Int.*, **73**, 8-14. <https://doi.org/10.1016/j.ndteint.2015.03.002>
- Lim, H.J., Kim, Y., Sohn, H., Jeon, I. and Liu, P. (2017), "Reliability improvement of nonlinear ultrasonic modulation based fatigue crack detection using feature-level data fusion",

- Smart Struct. Syst., Int. J.*, **20**(6), 683-696.
<https://doi.org/10.12989/sss.2017.20.6.683>
- Liu, P. and Sohn, H. (2016), "Numerical simulation of damage detection using laser-generated ultrasound", *Ultrasonics*, **69**, 248-258. <https://doi.org/10.1016/j.ultras.2016.03.013>
- Liu, P., Yang, S., Lim, H.J., Park, H.C., Ko, I.C. and Sohn, H. (2014), "Development of a wireless nonlinear wave modulation spectroscopy (NWMS) sensor node for fatigue crack detection", *Proceedings of SPIE*, Vol. 9064, 906406, San Diego, CA, USA.
- Liu, P., Sohn, H. and Park, B. (2015), "Baseline-free damage visualization using noncontact laser nonlinear ultrasonics and state space geometrical changes", *Smart Mater. Struct.*, **24**(6), 065036. <https://doi.org/10.1088/0964-1726/24/6/065036>
- Liu, P., Jang, J., Yang, S. and Sohn, H. (2018), "Fatigue crack detection using dual laser induced nonlinear ultrasonic modulation", *Opt. Laser Eng.*, **110**, 420-430. <https://doi.org/10.1016/j.optlaseng.2018.05.025>
- Mezil, S., Chigarev, N., Tournat, V. and Gusev, V. (2016), "Evaluation of crack parameters by a nonlinear frequency-mixing laser ultrasonics method", *Ultrasonics*, **69**, 225-235. <https://doi.org/10.1016/j.ultras.2016.04.005>
- Mikesell, T., van Wijk, K., Otheim, L., Marshall, H.P. and Kurbatov, A. (2017), "Laser ultrasound observations of mechanical property variations in ice cores", *Geosciences*, **7**(3), 47-65. <https://doi.org/10.3390/geosciences7030047>
- Monchalain, J.P., Aussel, J.D., Heon, R., Jen, C., Boudreault, A. and Bernier, R. (1989), "Measurement of in-plane and out-of-plane ultrasonic displacements by optical heterodyne interferometry", *J. Nondestruct. Eval.*, **8**(2), 121-133. <https://doi.org/10.1007/BF00565636>
- Murray, T., Deaton Jr, J. and Wagner, J. (1996), "Experimental evaluation of enhanced generation of ultrasonic waves using an array of laser sources", *Ultrasonics*, **34**(1), 69-77. [https://doi.org/10.1016/0041-624X\(95\)00090-P](https://doi.org/10.1016/0041-624X(95)00090-P)
- Noroy, M.H., Royer, D. and Fink, M. (1995), "Shear-wave focusing with a laser-ultrasound phased-array", *IEEE Trans. Ultrason. Ferroelect. Freq. Control*, **42**(6), 981-988. <https://doi.org/10.1109/58.476540>
- Park, B., Sohn, H., Yeum, C.M. and Truong, T.C. (2013), "Laser ultrasonic imaging and damage detection for a rotating structure", *Struct. Health Monit.*, **12**(5-6), 494-506. <https://doi.org/10.1177/1475921713507100>
- Park, B., Sohn, H., Malinowski, P. and Ostachowicz, W. (2017), "Delamination localization in wind turbine blades based on adaptive time-of-flight analysis of noncontact laser ultrasonic signals", *Nondestruct. Testing Eval.*, **32**(1), 1-20. <https://doi.org/10.1080/10589759.2015.1130828>
- Pierce, S., Culshaw, B. and Shan, Q. (1998), "Laser generation of ultrasound using a modulated continuous wave laser diode", *Appl. Phys. Lett.*, **72**(9), 1030-1032. <https://doi.org/10.1063/1.120955>
- Pistone, E., Li, K. and Rizzo, P. (2013), "Noncontact monitoring of immersed plates by means of laser-induced ultrasounds", *Struct. Health Monit.*, **12**(5-6), 549-565. <https://doi.org/10.1177/1475921713506767>
- Prada, C., Balogun, O. and Murray, T. (2005), "Laser-based ultrasonic generation and detection of zero-group velocity Lamb waves in thin plates", *Appl. Phys. Lett.*, **87**(19), 194109. <https://doi.org/10.1063/1.2128063>
- Saito, T., Matsuda, O., Tomoda, M. and Wright, O.B. (2010), "Imaging gigahertz surface acoustic waves through the photoelastic effect", *J. Opt. Soc. Amer. B*, **27**(12), 2632-2638. <https://doi.org/10.1364/JOSAB.27.002632>
- Scruby, C.B. and Drain, L.E. (1990), *Laser Ultrasonics Techniques and Applications*, CRC Press, Boca Raton, FL, USA.
- Sohn, H., Park, H.W., Law, K.H. and Farrar, C.R. (2007), "Combination of a time reversal process and a consecutiv outlier analysis for baseline-free damage diagnosis", *J. Intell. Mater. Syst. and Struct.*, **18**(4), 335-346. <https://doi.org/10.1177/1045389X0606629>
- Staszewski, W., Lee, B., Mallet, L. and Scarpa, F. (2004), "Structural health monitoring using scanning laser vibrometry: I. Lamb wave sensing", *Smart Mater. Struct.*, **13**(2), 251-260. <https://doi.org/10.1088/0964-1726/13/2/002>
- Staszewski, W., Lee, B. and Traynor, R. (2007), "Fatigue crack detection in metallic structures with lamb waves and 3D laser vibrometry", *Meas. Sci. Technol.*, **18**(3), 727. <https://doi.org/10.1088/0957-0233/18/3/024>
- van den Abeele, K.A., Johnson, P.A. and Sutin, A. (2000), "Nonlinear elastic wave spectroscopy (NEWS) techniques to discern material damage, part I: Nonlinear wave modulation spectroscopy (NWMS)", *J. Res. Nondestruct. Eval.*, **12**(1), 17-30. <https://doi.org/10.1080/09349840009409646>
- Wagner, J.W., McKie, A.D., Spicer, J.B. and Deaton, J.B. (1990), "Modulated laser array sources for generation of narrowband and directed ultrasound", *J. Nondestruct. Eval.*, **9**(4), 263-270. <https://doi.org/10.1007/BF00565644>
- Xu, B., Shen, Z., Ni, X. and Lu, J. (2004), "Numerical simulation of laser-generated ultrasound by the finite element method", *J. Appl. Phys.*, **95**(4), 2116-2122. <https://doi.org/10.1063/1.1637712>
- Yang, J., Liu, P., Yang, S., Lee, H. and Sohn, H. (2015), "Laser based impedance measurement for pipe corrosion and bolt-loosening detection", *Smart Struct. Syst., Int. J.*, **15**(1), 41-55. <https://doi.org/10.12989/sss.2015.15.1.041>
- Yashiro, S., Takatsubo, J., Miyauchi, H. and Toyama, N. (2008), "A novel technique for visualizing ultrasonic waves in general solid media by pulsed laser scan", *NDT & E Int.*, **41**(2), 137-144. <https://doi.org/10.1016/j.ndteint.2007.08.002>
- Yim, H.J., Park, S.J., Kim, J.H. and Kwak, H.G. (2016), "Evaluation of freezing and thawing damage of concrete using a nonlinear ultrasonic method", *Smart Struct. Syst., Int. J.*, **17**(1), 45-58. <https://doi.org/10.12989/sss.2016.17.1.045>
- Zaitsev, V.Y., Matveev, L. and Matveyev, A. (2009), "On the ultimate sensitivity of nonlinear-modulation method of crack detection", *NDT & E Int.*, **42**(7), 622-629. <https://doi.org/10.1016/j.ndteint.2009.05.001>

HJ